Local binding trend and local electronic structures of 4d transition metals

G. W. Zhang,* Y. P. Feng, and C. K. Ong
Department of Physics, National University of Singapore, Singapore 119260
(Received 7 May 1996; revised manuscript received 2 August 1996)

The local binding properties and electronic structures of $4d$ transition metals are studied by using a cluster model within the frame of density-functional theory. The equilibrium structures of all $4d$ transition-metal clusters are obtained by maximizing the binding energy of each cluster. The obtained mechanical properties, binding energies, and bond lengths well reproduced the trends displayed by corresponding set of bulk solids, which reveal that local interactions play a significant role in determining variations of binding properties of $4d$ transition metals. The bond lengths of clusters are found to converge more rapidly with cluster size toward their bulk limits than the binding energies. The relative stabilities of all clusters are discussed in terms of their ground-state electronic configurations. The contraction effect in valence-band widths (VBW's) is founded in clusters. The variation trend of VBW's for one cluster relative to another also bears analogs to the trend displayed by bulk solids. A striking correlation between magnetic moments and the magnitude of exchange splittings is found and elaborated. The mechanism leading to nonzero magnetizations and giant magnetic moments in some clusters is discussed in detail. [S0163-1829(96)04448-7]

I. INTRODUCTION

Recently, a lot of experimental and theoretical interest has been given to the investigation of unique electronic and magnetic properties of atomic clusters.[1–5] Among them, transition-metal clusters are of particular interest due to their promising practical applications in chemical industry and high-density magnetic record devices.[6,7] The efforts are mainly concentrated on the following aspects: (1) the ground-state geometries and relative structural stabilities;[8–11] (2) the evolution of cluster properties such as ionization potentials, binding energies, and so forth toward the bulk limits with the increase of the cluster size;[12–16] (3) magnetic properties and their dependence on cluster size, geometric symmetry, interatomic spacings, and applied magnetic fields;[17–21] (4) cluster chemistry including the reactivity, catalysis, etc.[7] Among those topics, one of the basic underlying questions is how the various properties of clusters change as the cluster size increases, and how many atoms it will take to reproduce the properties of a crystal.[22–27] However, little has been done concerning the property evolution with atomic numbers.

Actually, it is physically important to investigate the property evolution of transition-metal clusters with a fixed number of atoms and geometry as their atomic numbers change. It is also of physical importance to understand how the property trends of clusters compare with trends in the corresponding set of solids. The logical development of the investigation of the latter started with elemental isolated atoms,[28] closely condensed systems[29] to $3d$ transition-metal clusters. By using the linear-combination-of-atomic-orbitals molecular-orbital method within the scheme of density-functional theory, Painter calculated the binding energies and bond lengths of the $3d$ transition-metal clusters from Sc through Cu.[30] These clusters consist of only six atoms with octahedral symmetry. His calculations revealed that binding energies for small transition-metal clusters established a trend with atomic number which accurately reproduces the trend in cohesive energies which is exhibited by a corresponding set of crystalline solids. In a subsequent paper, Painter and Averill[31] used the same method to examine the trends in binding energies and interatomic spacings for all metallic clusters from hydrogen to copper. Their calculations further indicated that the variations of both binding energies and bond lengths for one metallic cluster relative to another are very similar to the relative variations of those of their bulk counterparts. Their results provided good insight into local metal-metal bonding characteristics which distinguish one metal from another. Regarding $4d$ transition metals, no systematic investigation of their local bonding trends and local electronic structure has been conducted by a cluster model, to the best of our knowledge.

In this paper, we calculated the binding energies, equilibrium interatomic spacings, and local electronic structures of $4d$ transition-metal clusters from Y through Cd by using a linear-combination-of-atomic-orbitals molecular-orbital approach within the frame of density-functional theory. The main object of this work is to understand how cluster properties relate to one another and to their bulk limit while progressing from one element to another, which is basically similar in spirit to Painter's work. In order to reduce the size and structure effects on the cluster properties, we chose clusters with only six atoms and octahedral symmetry as in the case of Painter. The whole paper is arranged as follows. In Sec. II, we describe the theory and computational methods. In Sec. III, we concentrate on discussing the local binding trends, local electronic structure, and the giant magnetic moments of clusters. Finally, we summarize our results in Sec. IV.

II. THEORY AND METHODS

Our calculations are based on the density-functional theory to which the local spin-density approximation is adapted.[32] Within this frame, the ground-state properties of the clusters can be well described by Kohn-Sham (KS) equations. The spin-dependent exchange-correlation potential

presented in KS equations is approximated in the Barth-Hedin form.[33] The linear-combination-of-atomic-orbitals method is used to obtain molecular wave functions of the clusters. Throughout our calculations, numerical atomic wave functions of $4d$, $5s$, and $5p$ are used as the basis set. The inner orbitals such as $1s$, $2s$, etc. are kept frozen in order to reduce the computational efforts. The KS equations are solved self-consistently using the discrete variational method, which has been discussed in detail by Ellis *et al.*[34] Using the solutions of KS equations, the total energy of the clusters can be readily obtained and the binding energy can be calculated from $E_b = E_{\rm tot} - E_{\rm ref}$, where $E_{\rm tot}$ is the total energy of the cluster and $E_{\rm ref}$ is the sum of the total energy of the free atom. The equilibrium structures of the clusters are obtained by maximizing the binding energy E_b with respect to the interatomic spacings. The Mulliken population analysis has been used to obtain the occupation numbers of atomic orbitals. The magnetic moments are defined as the differences of occupation number between the spin-up and spin-down states. The partial density of states (DOS) of the spin σ is obtained by expanding each discrete energy level according to Lorentzian formula

$$D^{\alpha}_{nl\sigma}(E) = \sum_i A^{\alpha}_{nl\sigma i} \frac{\delta/\pi}{(E-\varepsilon_{i\sigma})^2 + \delta^2}, \tag{1}$$

where i is the index of energy level and σ is the spin index. $A^{\alpha}_{nl\sigma i}$ is the Mulliken population of atomic orbital of atom α. The total density of states of the spin σ is defined as the sum of the partial density of states:

$$D_{\sigma}(E) = \sum_{nl\alpha} D^{\alpha}_{nl\sigma}(E). \tag{2}$$

The vertical ionization potentials (IP's) of clusters are calculated self-consistently in terms of transition-state scheme, which automatically takes into consideration electron relaxations.

III. RESULTS AND DISCUSSIONS

A. Local binding properties

We calculated the binding energy of each $4d$ transition-metal cluster while keeping the octahedral symmetry constraint and allowing the clusters to relax radially. The binding energy as a function of the parameter D is shown in Fig. 1, where D is the distance between the center of the cluster and its vertex. For each curve presented in Fig. 1, there is an energy minimum which corresponds to the equilibrium geometric configuration. The obtained values of binding energies (eV/atom), D (a.u.), ionization potentials (eV), and magnetic moments (μ_B atom) are listed in Table I. From the binding-energy curves depicted in Fig. 1, we may derive a broad spectrum of mechanical properties of the clusters studied. First, the Cd cluster has a much smaller binding energy and a much larger equilibrium interatomic spacing in comparison with those of the midrow members such as Nb, Tc, Ru, and so on. The Y cluster also exhibited a relatively large interatomic spacing and a relatively small binding energy. We may conclude that the Y and Cd clusters are weakly bonded, which well reproduces the bonding properties of the corresponding bulk solids. On the other hand, the midrow members such as Nb, Tc, Ru, Mo clusters all display relatively small interatomic spacings and relatively large binding energies, which indicates that those clusters are strongly bonded. Therefore, it is apparent in results of our calculations that the clusters bear analogs to the corresponding bulk solids in the aspects of bonding strengths and equilibrium interatomic spacings. Second, the slope of the energy curve determines the restoring force on the displaced atom and elastic properties of respective cluster. From Fig. 1, we find that the energy curves of members at both ends along the $4d$ series in the Periodic Table (for example, Y, Cd, Zr, and Ag) are flat, in strong contrast with those of the midrow members such as Nb, Tc, Mo, Ru clusters, whose energy curves are sharp. The energy curves of Rh and Pd fall between these extremes. Accordingly, it is also apparent from the results of our calculations that a qualitative correspondence exists between clusters and their bulk counterparts in the aspect of

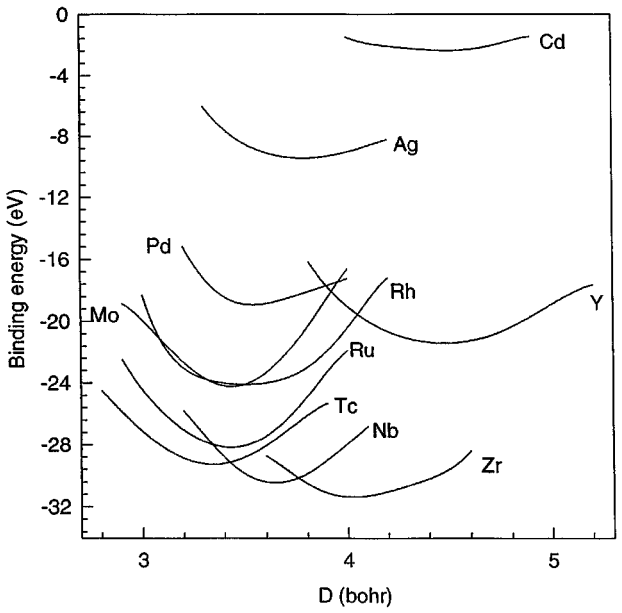

FIG. 1. The binding energy for $4d$ transition-metal clusters as a function of the distance from the center of the cluster to its vertex.

TABLE I. The binding energy (E_b), the displacement from the center of cluster to its vertex (D), ionization potentials (IP's) of $4d$ transition-metal clusters, and averaged magnetic moment (m) per atom.

Cluster	E_b (eV)	D (a.u.)	IP (eV)	m (μ_B)
Y_6	3.53	4.40	6.22	0.00
Zr_6	5.23	3.96	5.86	0.33
Nb_6	5.07	3.64	7.40	0.67
Mo_6	4.05	3.40	7.27	0.33
Tc_6	4.91	3.36	6.88	0.33
Ru_6	4.70	3.40	7.11	1.00
Rh_6	4.03	3.48	7.42	0.99
Pd_6	3.14	3.50	7.73	0.00
Ag_6	1.56	3.76	8.04	0.33
Cd_6	0.39	4.48	6.91	0.00

elastic properties. Finally, the second derivative of the energy curve determines the bulk modulus of each cluster if we define the cluster's bulk modulus in the same way as those of the bulk crystalline solids. Both experimental measurements and theoretical calculations indicated that the bulk modulus of the early $4d$ transition metals increase with the increase of atomic number and those of the late $4d$ transition metals decrease with the increase of the atomic number.[29] Among these members, Ru and Tc which are located at the center of the $4d$ series have the largest values of 3.21 and 2.97, respectively, and Y and Cd which lie at the ends of $4d$ series have the smallest values of 0.366 and 0.467, respectively (all in units of 10^{11} N/m^2), with those of Zr, Nb, Mo, Rh, Pd, and Ag falling between these extremes. From Fig. 1, we can infer that the bulk modulis of Y through Cd clusters generally exhibit the same trends as their corresponding bulk crystalline solids.

In order to investigate the binding trends with atomic number and convergence of the clusters' binding energies toward those of their bulk values, we plotted the binding-energy curves of bulk solids including experimental measurements and results of band-structure calculations in Fig. 2(a).[29,35,36] The binding-energy curves of clusters are also presented in Fig. 2(a) for comparison. Experimental values for crystalline solids are denoted by solid circles. Calculated band-structure values for crystalline solids are represented by solid squares, and solid triangles stand for the calculated values of clusters. From Fig. 2(a), the binding energy of each cluster is smaller than that of the measured value of the corresponding crystalline solid. The absolute differences between energy values for the corresponding elements of the bulk and cluster systems vary from 0.75 to 2.77 eV per atom. Comparing the energy values of local-density approximation (LDA) band-structure calculations on the crystalline solids with the energy values of present LDA cluster calculations on the cluster systems, we find that the energy differences between corresponding midrow elements of bulk and cluster systems such as Nb, Mo, Tc, and Ru are as high as about 2.7 eV per atom, for the early members such as Y and Zr, their energy differences are about 1.4 eV per atom, for the late members such as Pd, Ag, and Cd, their energy differences are 0.54, 1.32, and 1.01 eV per atom. Although band-structure calculations tend to overestimate the cohesive energy in most cases, the results from band-structure calculations show closer agreement with experimental results than results from present cluster calculations. Therefore, it is reasonable to infer that the cluster binding energy will converge to the bulk LDA results as the sizes of clusters increase. However, for the discussion of the binding trends, it is not the absolute differences but the relative differences that play a significant role. From Fig. 2(a), we may find that although the absolute energy differences between corresponding elements of cluster and bulk systems are large, these differences are actually slowly varying. So, the trend exhibited by experimental binding energies is well reproduced by the clusters as small as six atoms across the whole $4d$ transition-metal series. Of course, there is a small deviation from the experimental trend for Nb cluster. For the experimental case, its binding energy is somewhat bigger than that of both its left-hand neighbor Zr and its right-hand neighbor Mo; however, for the case of clusters, its binding energy is smaller

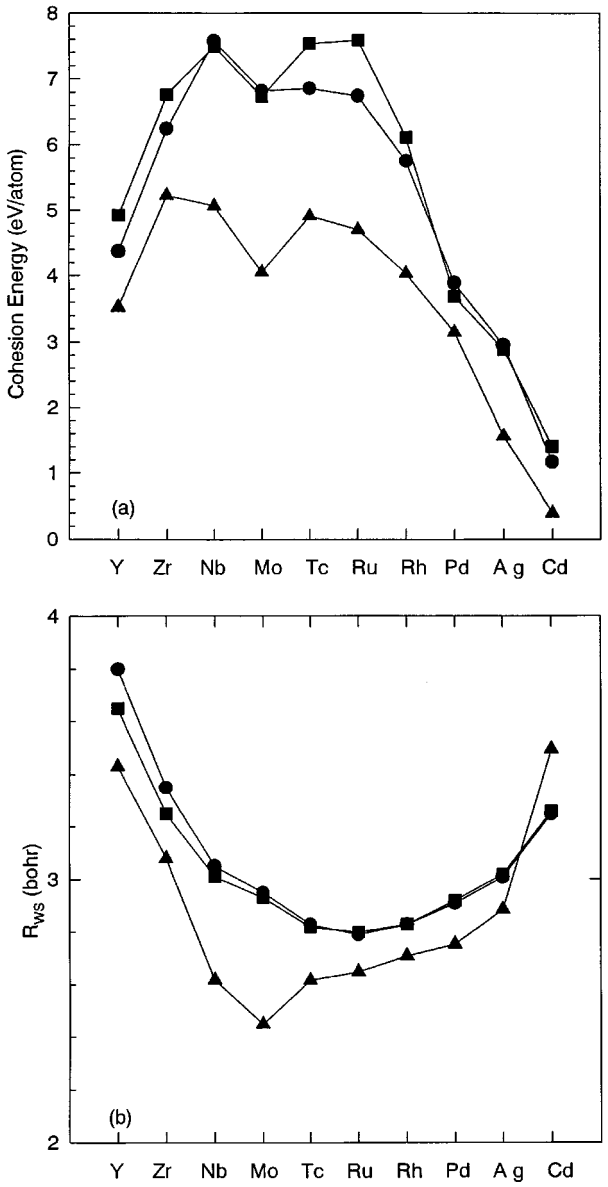

FIG. 2. A Comparison of (a) crystalline and cluster binding energies and (b) crystal and cluster Wigner-Seitz radii. Solid squares denote experimental bulk cohesive energies. Solid circles and triangles stand for bulk cohesive energies from LDA band-structure calculations and present cluster binding energies, respectively.

than that of its left-hand neighbor Zr even though its binding energy is still larger than that of its right-hand neighbor Mo. Because this deviation is not presented in the energy curve of the LDA band-structure calculations for the corresponding crystalline bulk, the origin of this discrepancy in the trend cannot simply be attributed to the local-density approximation itself. This discrepancy probably originated with the relatively large magnetization of Nb because magnetization will lower the total energy of the system. Nb has a magnetic moment of $0.67\mu_B$, which is twice that of Zr (0.33).

In Fig. 2(b), we plotted the Wigner-Seitz radii of the crystalline solids including results from experimental measurements and LDA band-structure calculations.[29,35,36] These values are denoted by solid squares and solid circles,

TABLE II. The calculated data of ground-state electronic structure and ground-state electronic configurations for $4d$ transition-metal clusters.

Clusters	HOMO eV	LUMO eV	VBW eV	Symbols	HOMO electrons	configurations
Y	−4.02	−3.77	3.41	Bu ↑	1	closed
Zr	−3.83	−3.66	4.55	$T2u$ ↑	2	open
Nb	−4.99	−4.79	5.06	$T1u$ ↓	2	open
Mo	−5.10	−4.93	5.94	$T1g$ ↑	2	open
Tc	−4.08	−4.03	7.05	Eu ↑	2	closed
Ru	−4.27	−4.15	6.73	Eg ↓	1	open
Rh	−4.54	−4.51	5.93	Eg ↓	2	closed
Pd	−8.65	−8.50	5.10	$T2g$ ↑	3	closed
Ag	−5.63	−3.29	6.45	$T2u$ ↓	1	open
Cd	−4.79	−3.25	8.97	Eg ↑	2	closed

respectively. The calculated equilibrium cluster bond lengths are listed in Table I. In order to make a comparison with the Wigner-Seitz radii from LDA band-structure calculations and experimental measurements, we converted the equilibrium bond lengths of clusters to corresponding Wigner-Seitz radii by formulas such as $R_{\mathrm{WS}}=2D/(16\pi/3)^{1/3}$ and $R_{\mathrm{WS}}=\sqrt{2}D/(8\pi/3)^{1/3}$,[30,31] where D is the displacement between the cluster center and its vertex. The first formula is suited to fcc crystals [the symmetry adopted by Morruz *et al.* for all $4d$ transition metals except Nb and Mo (Ref. 29)], and the second is applicable to bcc crystals (Nb and Mo only). The resultant values for the cluster Wiggner-Seitz radii are presented in Fig. 2(b) and indicated by the solid triangles. From Fig. 2(b), we find that bond lengths of the clusters contract in comparison with both experimental and theoretical values for the corresponding crystalline solids with the only exception of the Cd cluster, whose bond length is somewhat larger than its corresponding bulk value. The bond-length contractions relative to calculated bulk parameters are as small as about 5% for all elements except Nb and Mo of which the bond-length contraction reaches about 12%. This kind of contraction effect is not unique to the $4d$ transition-metal clusters. It was also found in other metal clusters,[37] which embodies the dominant role of near-neighbor interactions in determining the lattice constants. As far as the bonding trend is concerned, the cluster results reproduced the trend of LDA Wigner-Seitz radii of crystalline solids especially well. However, there is a noticeable deviation from the LDA band-structure calculations in the Mo-Tc sequence. This discrepancy is understandable because in the implementation of LDA band-structure calculations, Moruzzi *et al.* adopted bcc structures for Mo and Nb but a fcc structure for Tc and other elements. However, in the present cluster calculations, we retained regular octahedral symmetry for both Mo and Nb clusters without the tetragonal distortion characteristic of the octahedral fragment of the bcc lattices.

As mentioned above, elastic properties, bulk modulus, binding energies, and bond lengths of small $4d$ transition-metal clusters well reproduced the trends exhibited by corresponding crystalline solids. This kind of property correlation between clusters and solids is closely related to a strong d character in their valence states, and to their progressive filling of $4d$ shells while going from left to right along the $4d$ series in the Periodic Table. First, based on the Mott-Slater model,[38] the binding nature of transition metals is mainly determined by their d electrons; other factors such as s electrons and magnetism are only details of secondary importance. Second, compared with the other sp valence orbitals with comparable energy, $4d$ orbitals are much more concentrated. Their much smaller numbers of spherical nodal surface allow them to decrease exponentially. As a result, they are fairly localized; they can neither be strongly perturbed by the lattice potential nor overlap very strongly with states of other atoms. So neighbor interactions play a dominant role in determining their properties. That is why a cluster with a small number of atoms can well reproduce the binding properties of corresponding sets of solids. Finally, from Fig. 2(a), we can observe that the energy curves are nearly parabolic for both clusters and solids. This is a consequence of the change from bonding to antibonding character of d orbitals. For the materials at the beginning of the transition-metal series, the bonding orbitals are being filled. The more the bonding orbitals are being filled, the bigger the binding energy will be. This is simply because the mechanical attraction will increase while more and more bonding orbitals are filled. The effect is maximized near the middle of the $4d$ transition-metal series, when the bonding orbitals are filled; then the trend is reversed, and the antibonding orbitals begin to be filled.

B. Local electronic structures

In this section we will concentrate on the investigation of the local ground-state electronic structure of $4d$ transition metals. The obtained results are listed in Table II, where B, E, and T are symbols of the one-dimensional, two-dimensional, and three-dimensional irreducible representations of the point group with octahedral symmetry. g and u stand for even and odd, respectively. Up and down arrows presented in Table II represent up and down spins, respectively. From Table II, we find that the gap between highest occupied molecular orbitals (HOMO's) and lowest unoccupied molecular orbitals (LUMO's) displays large variations through the entire $4d$ series. Ag and Cd clusters have gaps as large as 2.34 and 1.54 eV, respectively. In contrast, Tc has a quite small gap of 0.05 eV. The gaps for other members have

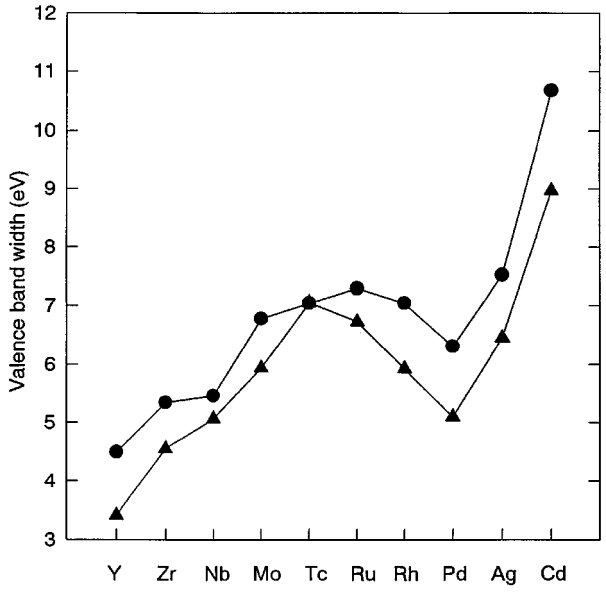

FIG. 3. A comparison of crystal and cluster valence-band width. Solid triangles represent the results from LDA band-structure calculations. Solid triangles stand for present results for clusters.

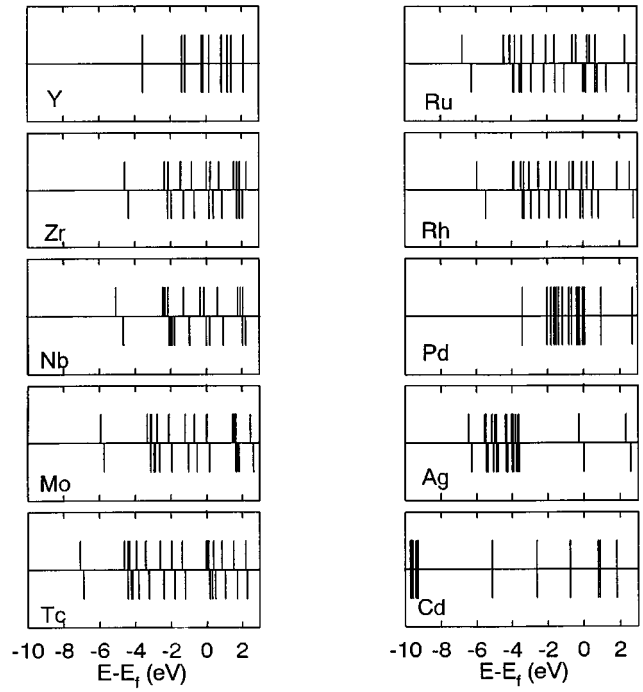

FIG. 4. The energy spectra of 4*d* transition-metal clusters. Fermi energy levels are shifted to zero. The upper panel is the result of spin-up band, and the lower the result of spin-down band.

a magnitude of 0.1–0.3 eV, falling between foregoing extreme cases. Actually, there exists no explicit correction between atomic number and gap.

For a cluster, its electron number in the HOMO plays a significant role in determining its ground-state electronic configuration. From Table II, we may find that HOMO's of Nb, Ru, Rh, and Ag clusters are all occupied by up spin electrons, and those for Y, Zr, Mo, Tc, Pd, and Cd clusters are occupied by down spin electrons. This picture is quite different from that obtained for 3*d* clusters of which the HOMO's are always occupied by up-spin electrons. On the other hand, the ground-state electronic configuration of a cluster determines its relative structural stability. From Table II, we can see that Y, Tc, Rh, Pd, and Cd clusters have a fully occupied HOMO which leads to a ground state with a closed electronic shell. Thus these clusters are reasonably expected to be quite stable. However, for the Zr, Nb, Mo, Ru, and Ag clusters, each has an unfilled HOMO which leads to a ground state with an open electronic shell. Hence, they are apt to undergo the Jahn-Teller distortion which may lower the cluster's symmetry so as to reduce the degeneracy of its ground state and finally lower its energy.

Another interesting result of calculations is that there is a striking correlation between the valence-band width (VBW) of clusters and that of corresponding crystalline solids. The obtained VBW data for the 4*d* transition-metal clusters are listed in Table I. In Fig. 3, we plotted the VBW curves for both cluster and crystalline systems for comparison, where solid circles stand for the former and solid triangles for the later.[29] From Fig. 3, we can see that the VBW of clusters are smaller than that of corresponding crystalline solids with the only exception of Tc cluster of which the VBW is nearly the same as that of its crystalline solid. Here again, the trend in the VBW of LDA band structure is rather well reproduced by the clusters' VBW. Progressing from Y through Cd, a deviation from the LDA band-structure calculations only occur at Tc. Hence, the VBW difference for one metal relative to another is very accurately represented by the small octahedral clusters.

In Fig. 4, we plotted the eigenvalue spectra for all the clusters from Y through Cd. In each case, the Fermi level is shifted to zero. The upper panel of each diagram is the eigenvalue spectrum of up-spin electrons, and the lower panel the eigenvalue spectrum of down-spin electrons. From Fig. 4, we can see that there are no exchange splittings between up- and down-spin bands for Y, Pd, and Cd clusters. The other clusters exhibited exchange splitting at varying degrees with Nb, Ru, and Rh having the largest magnitude of exchange splittings. Referring to Table I where we listed the averaged magnetic moments per atom of each clusters, one can find that Y, Pd, and Cd clusters carried no magnetic moments. However, Ru, Rh, and Nb clusters sustained magnetic moments as large as 1.0, 0.99, and 0.67 (μ_B/atom), respectively. Therefore, there is a striking correlation between the cluster magnetic moment and its magnitude of exchange splittings. The larger the magnitude of exchange splitting of a cluster, the larger the magnetic moment of the cluster. It is understandable because the exchange splitting may cause a shift of the spin-up band relative to spin-down band, and this shift may result in a different occupation of spin-up states and spin-down states. The net difference of electron number between spin-up and spin-down states determine the magnitude of magnetic moments of the whole clusters. So generally, the larger the exchange splitting, the larger the magnetic moment.

C. Giant magnetic moments

Magnetic properties of all clusters from Y through Cd will also prove topical for the discussion. From Table I, we

may find that each cluster except Y, Pd, and Cd carries a finite magnetic moment, with Ru and Rh clusters having giant magnetic moments of 1.0 and 0.99 (μ_B/atom), respectively. This picture is quite different from the magnetic behaviors of their bulk solids. Although $4d$ transition metals all have unfilled localized d electronic shells, none of them are magnetic. This nonzero magnetization phenomenon is not unique to the $4d$ clusters. Recent calculations have predicted magnetic ordering in $3d$ clusters whose corresponding bulk materials are normally nonmagnetic.[39–40] Most predicted nonzero magnetizations have been confirmed later by Stern-Gerlach experiments.[41–43] There exists a consensus that the nonzero magnetization in clusters whose bulk materials are nonmagnetic or enhanced magnetic moments in clusters whose bulk counterparts are already magnetic is due to the clusters' lower dimensionality and higher symmetry.[40]

Before discussing the origin of the giant magnetic moments of Ru_6 and Rh_6 clusters, we first review other predictions of giant magnetic moments of Ru and Rh clusters with a cluster size larger than six atoms. Galicia calculated magnetic properties of Rh_{13} cluster with octahedral symmetry using a molecular-orbital approach.[44] Because he adopted a fcc crystal structure and bulk interatomic spacing for the Rh_{13} cluster, his calculation actually was performed on a relatively larger fragment of bulk rhodium. Based on his spin-polarized calculations, he predicted a magnetic moment of 1.0 (μ_B/atom) which is the same as our result for octahedral Rh_6 cluster. Reddy, Khanna, and Dunlap[40] calculated the magnetic moment of Ru_{13} cluster with icosahedral symmetry, and predicted a giant magnetic moment of 1.02 (μ_B/atom), which is also in the same order of the magnetic moment obtained for Ru_6 cluster. In fact, the predicted giant magnetic moments for both Ru and Rh clusters were later confirmed by the Stern-Gerlach experiment.[45]

In order to understand the origin of the giant magnetic moments of Ru_6 and Rh_6 clusters, we depicted eigenvalue spectra as well as the total density of states, sp and d partial density of states of these clusters in Figs. 4 and 5. Figures 5(a) and 5(b) are results of Ru and Rh clusters, respectively. Vertical dashed lines in Fig. 5 represent Fermi energy levels which are shifted to zero. The upper panel stands for the DOS of up spin, and the lower panels represent down spin. The solid lines, dashed lines, and dotted-dashed lines stand for the total DOS, $4sp$ partial DOS, and $4d$ partial DOS, respectively. From Fig. 5 we can see that the total DOS for both Ru and Rh clusters show a very large peak near the top of the valence band, and Fermi energy levels (E_f) lie near the large peak. This is different from their bulk counterparts of which Fermi energy levels lie in a dip of DOS. This high DOS contributes a lot to the giant magnetic moments because a small shift between two large peaks may result in a non-negligible difference between up- and down-spin electrons. In addition, as mentioned before, the magnitude of the magnetic moments of cluster is obviously correlated with the degrees of exchange splitting between up-spin and down-spin bands. The larger the exchange splitting, the larger the magnetic moments. Figure 4 shows that both Ru and Rh have large exchange splittings between their spin-up and spin-down bands. The magnitude of these exchange splittings is of the order of 0.5 eV for the sp band and 0.7 eV for the d band. The obtained magnitude of exchange splittings of the present calculations is very close to the result of Galicia who obtained an exchange splitting of 0.6 eV.

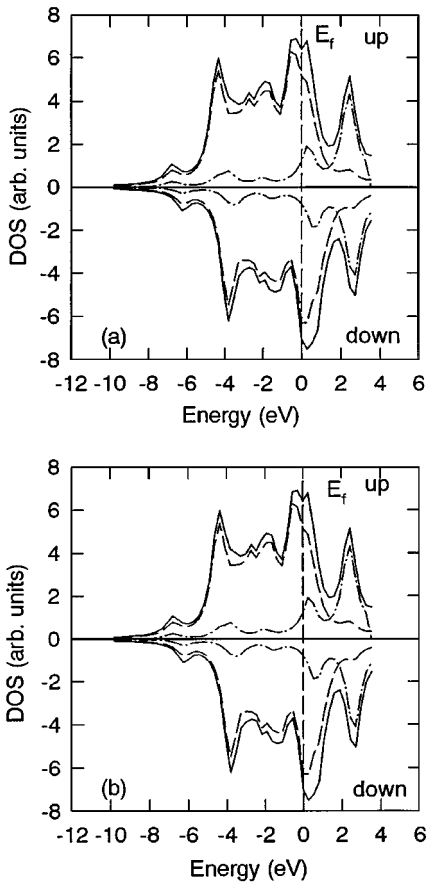

FIG. 5. Total density of states (solid lines), d partial density of states (dashed lines), and sp partial density of states (dotted dashed lines) for (a) Ru cluster and (b) Rh cluster. Up and down denote spin up and spin down.

Finally, it is worth mentioning the following. (1) There are two factors which contribute to the high DOS near the Fermi energy levels. First, the VBW of the cluster is narrower than that of its bulk solid due to its reduced dimensionality. The same number of electrons filling a narrower band will necessarily result in a higher density of states. Second, the high symmetry adopted in our calculations produced a large averaged degeneracy. So the same energy interval may accommodate more isospin electrons for the system with larger averaged degeneracy. (2) The DOS is mainly contributed to by d electrons. s and p electrons make a small fraction of the contribution to the total DOS, which can be seen from Figs. 5(a) and 5(b).

IV. CONCLUDING REMARKS

To sum up, we have made systemmatic investigations of the mechanical, electronic, and magnetic properties of all $4d$ transition metals from Y through Cd by a cluster model. All our studies are carried out within the scheme of density-functional theory to which local spin-density approximation has been added. The equilibrium structures of the clusters were obtained by maximizing the binding energy with respect to interatomic spacings. The binding energies for all

clusters studied are smaller than those of their corresponding bulk solids. The mechanical properties such as elasticity and bulk modulus, binding energies, and bond lengths of clusters well reproduced the trends exhibited by their bulk counterparts. However, we find that bond lengths are more rapidly convergent with cluster size than binding energy. Concerning local electronic structure, we find that VBW's of all clusters are smaller than the corresponding crystalline solids, except the Tc cluster of which the cluster VBW is almost the same as that of its crystalline solid. Based on our calculations, it is apparent that the clusters bear analogs to the corresponding solids in the aspect of the variations of VBW's for one element relative to another. We also find a striking correlation between cluster magnetic moments and the magnitude of exchange splittings. The larger the magnitude of exchange splittings, the larger the magnetic moments. Nonzero magnetizations are found for some $4d$ clusters; in particular giant magnetic moments are found for Ru and Rh clusters. The mechanism leading to nonzero magnetizations and giant magnetic moments is discussed in detail. The relative stabilities of clusters are analyzed in terms of their ground-state electronic configurations, too.

*Author to whom correspondence should be addressed. Electronic address: scip5095@leonis.nus.sg

[1] Proceedings of the Sixth International Meeting on Small Particles and Inorganic Clusters, Chicago, 1992 [Z. Phys. D **26** (1993)].
[2] W. A. deHeer, Rev. Mod. Phys. **65**, 611 (1993).
[3] M. Brack, Rev. Mod. Phys. **65**, 677 (1993).
[4] S. Sugano, *Microcluster Physics* (Springer, Berlin, 1991).
[5] *Clusters and Cluster-Assembled Materials*, edited by R. S. Averback, J. Bernholc, and D. L. Nelson, MRS Symposia Proceedings No. 206 (Materials Research Society, Pittsburgh, 1991).
[6] R. W. Chantrell and K. O. Grady, *The Magnetic Properties of Fine Particles in Applied Magnetism* (Kluwer, Dordrecht, 1994).
[7] D. R. Salahub and N. Russo, *Metal-Ligand Interactions: From atoms, to Clusters, to Surfaces* (Kluwer, Dordrecht, 1992).
[8] T. H. Upton, Phys. Rev. Lett. **56**, 2168 (1986).
[9] M. Menon and K. R. Subbaswamy, Phys. Rev. B **50**, 11 577 (1994); **51**, 17 952 (1995).
[10] M. J. Lopez, P. A. Macros, and J. A. Alonso, J. Chem. Phys. **104**, 1056 (1996).
[11] U. Rothlisberger and W. Adreoni, Chem. Phys. Lett. **198**, 478 (1992).
[12] Shihe Yang and M. B. Knickelbein, J. Chem. Phys. **93**, 1553 (1990).
[13] E. A. Rohlfing, D. M. Cox, and A. Kaldor, K. H. Johnson, J. Chem. Phys. **81**, 3864 (1984).
[14] J. P. Perdew, Phys. Rev. B **37**, 6175 (1988).
[15] B. K. Rao and P. Jena, J. Phys. F **16**, 461 (1986).
[16] M. E. Garcia, G. M. Pastor, and K. H. Bennemann, Phys. Rev. Lett. **67**, 1142 (1991).
[17] B. I. Dunlap, Phys. Rev. A **41**, 5691 (1990).
[18] G. W. Zhang, Y. P. Feng, and C. K. Ong Z. Phys. D (to be published).
[19] D. C. Douglass, A. J. Cox, J. P. Bucher, and L. A. Bloomfield, Phys. Rev. B **47**, 12 874 (1993).
[20] A. J. Cox, J. G. Louderback, and L. A. Bloomfield, Phys. Rev. Lett. **71**, 923 (1993).
[21] S. N. Khanna and S. Linderoth, Phys. Rev. Lett. **67**, 742 (1991).
[22] P. A. Montano, G. K. Shenoy, E. E. Alp, W. Schulze, and J. Urban, Phys. Rev. Lett. **56**, 2076 (1986).
[23] B. K. Rao, S. N. Khanna, and P. Jena, Phys. Rev. B **36**, 953 (1987).
[24] J. D. Kress, M. S. Stave, and A. E. DePristo, J. Chem. Phys. **93**, 1556 (1989).
[25] K. Raghaven, M. S. Stave, and A. E. Depriato, J. Chem. Phys. **91**, 1904 (1989).
[26] B. Delley, D. E. Ellis, A. J. Freeman, E. J. Baerends, and D. E. Post, Phys. Rev. B **27**, 2132 (1983).
[27] K. Rademann, O. Dimopoulou-Rademann, M. Schlauf, U. Even, and F. Hensel, Phys. Rev. Lett. **69**, 3208 (1992).
[28] F. Herman and S. Skillman *Atomic Structure Calculations* (Prentice-Hall, Englewood Cliffs, NJ, 1963).
[29] V. L. Moruzzi, J. F. Janak, and A. R. Williams, *Calculated Electronic Properties of Metals* (Pergamon, New York, 1978).
[30] G. S. Painter, Phys. Rev. Lett. **70**, 3959 (1993).
[31] G. S. Painter and F. W. Averill, Phys. Rev. B **50**, 5545 (1994).
[32] For a review, see J. Callaway *et al.*, in *Solid State Physics*, edited by H. Ehrenreich *et al.* (Academic, New York, 1984).
[33] U. von. Barth and L. Hedin, J. Phys. C **5**, 1629 (1972).
[34] D. E. Ellis and G. S. Painter, Phys. Rev. B **2**, 2887 (1970).
[35] J. F. Janak and A. R. Williams, Phys. Rev. B **14**, 4199 (1976).
[36] C. Kittel, *Introduction to Solid State Physics* (Wiley, New York, 1976).
[37] B. K. Rao, S. N. Khanna, and P. Jena, Phase Transitions **24-26**, 35 (1990).
[38] F. Gautier, *Structure and Cohesion of Transition Metals and Alloys in Physics of Modern Materials* (IAEA, Autria, 1980), Vol. II.
[39] B. I. Dunlap, Z. Phys. D **19**, 255 (1991).
[40] B. V. Reddy and S. N. Khanna, and B. I. Dunlap, Phys. Rev. Lett. **70**, 3323 (1993).
[41] D. M. Cox, D. J. Trevor, R. L. Whetten, E. A. Rohlfing, and A. Kaldor, Phys. Rev. B **32**, 7290 (1985).
[42] J. P. Bucher, D. C. Douglass, and L. A. Bloomfield, Phys. Rev. Lett. **66**, 3052 (1991).
[43] I. M. L. Billas, J. A. Becker, A. Chatelain, and W. A. deHeer, Phys. Rev. Lett. **71**, 4067 (1993).
[44] R. Galicia, Rev. Mex. Fis. **32**, 51 (1985).
[45] A. J. Cox, J. G. Louderback, S. E. Apsel, and L. A. Bloomfield, Phys. Rev. B **49**, 12 295 (1994).